

# Communications with guaranteed bandwidth and low latency using frequency-referenced multiplexing

Received: 14 April 2022

Accepted: 26 July 2023

Published online: 28 August 2023

 Check for updates

Zichuan Zhou<sup>1</sup>, Jinlong Wei<sup>2</sup>✉, Yuan Luo<sup>3</sup>✉, Kari A. Clark<sup>1</sup>, Eric Sillekens<sup>1</sup>, Callum Deakin<sup>1</sup>, Ronit Sohanpal<sup>1</sup>, Radan Slavik<sup>4</sup> & Zhixin Liu<sup>1</sup>✉

Emerging cloud applications such as virtual reality and connected car fleets demand guaranteed connections, as well as low and stable latency, to edge data centres. Currently, user–cloud communications rely on time-scheduled data frames through tree-topology fibre networks, which are incapable of providing guaranteed connections with low or stable latency and cannot be scaled to a larger number of users. Here we show that a frequency-referenced multiplexing method can provide guaranteed bandwidth and low latency for time-critical applications. We use clock and optical frequency synchronization, enabled by frequency comb and signal processing techniques, to provide each user with dedicated optical bandwidth, creating scalable user–cloud upstream communications. As a proof of concept, we demonstrate a frequency-division multiplexing system servicing up to 64 users with an aggregate bandwidth of 160 GHz, exhibiting a data rate of up to 4.3 Gbps per user (240.0 Gbps aggregated capacity considering a 200 GHz wavelength band) with a high receiver sensitivity of  $-35$  dBm.

The number of virtual reality (VR) devices, augmented reality (AR) devices and intelligent autonomous vehicles are expected to rapidly increase in the next decade (Fig. 1), leading to a substantial growth in global data traffic<sup>1,2</sup>. In contrast to the applications of conventional data traffic (such as video streaming), these emerging cloud applications demand guaranteed connections (rather than very high band rate), as well as low and stable latency to edge data centres (Table 1)<sup>3–6</sup>. The development of these devices, thus, creates distinct requirements for future user–cloud communication infrastructures, which are related to availability, precision, scalability, flexibility and compatibility.

Specifically, the infrastructures should provide guaranteed connections with stable and low latency, where the physical link between the user and the cloud is preferably a dedicated channel such that

uncertainty due to scheduling is eliminated, enabling precise time dissemination through the telecom infrastructure.

They should provide an accurate and synchronized clock to enable sub-nanosecond time synchronization. VR and self-driving car fleets require, for example, low-cost and highly scalable time synchronization infrastructure to deliver sub-metre-scale positioning of devices<sup>7</sup>. Although sub-nanosecond time synchronization is achievable using GPS, it is costly and relies on line of sight to the sky, which can be difficult or impossible, for example, when underground or within buildings<sup>8</sup>, and can be inhibited by, for example, atmospheric ash following volcanic eruptions<sup>9</sup>. Therefore, sub-nanosecond time synchronization through the already deployed optical fibre access networks is highly desired.

<sup>1</sup>Department of Electronic and Electrical Engineering, University College London, London, UK. <sup>2</sup>Peng Cheng Laboratory, Shenzhen, China. <sup>3</sup>School of Science and Engineering, Shenzhen Institute of Artificial Intelligence and Robotics for Society, The Chinese University of Hong Kong, Shenzhen, China. <sup>4</sup>Optoelectronic Research Centre, University of Southampton, Southampton, UK. ✉e-mail: [weijl01@pcl.ac.cn](mailto:weijl01@pcl.ac.cn); [luoyuan@cuhk.edu.cn](mailto:luoyuan@cuhk.edu.cn); [zhixin.liu@ucl.ac.uk](mailto:zhixin.liu@ucl.ac.uk)

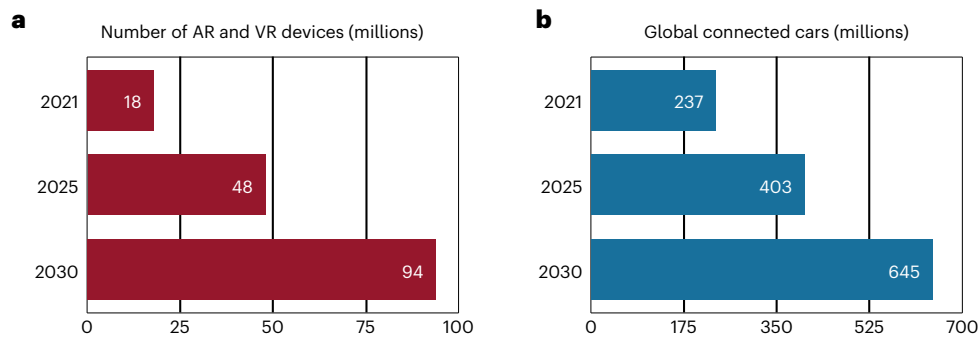


**Fig. 1 | Trends in global increase in VR/AR devices and connected car fleet.**

**a**, Estimated number of consumer human–machine interface devices dedicated to VR and AR in major areas including the United States, Europe, China and Japan. The estimation suggests a booming of AR/VR applications, with an average annual growth rate (AAGR) of about 28% from 2021 to 2025, followed by a continuously strong AAGR of about 14% from 2025 to 2030. The VR/AR devices support time-critical applications such as remote surgery, immersive

education, teleconference, online gaming and industrial designs<sup>55</sup>. **b**, Estimations summarized as collected by PricewaterhouseCoopers and Strategy&<sup>56</sup>, showing an increase in connected cars in operation to 403 million by 2025, featuring an AAGR of 14% from 2021 to 2025, followed by an AAGR of 10%, reaching 645 million by 2030. These estimates account for the largest geographical countries for connected cars, namely, the United States, Europe, China and Japan.

The guaranteed connections should then be scalable to support a large number of end-user devices. The next decade will potentially see a quintuple increase in user devices (Fig. 1), and thus future access network should, ideally, provide the availability and precision for a quintupled number of users.

The per-user data rate should be flexibly configured, each at a data rate of a few gigabits per second (Gbps) (Table 1)<sup>10,11</sup> to support different types of service<sup>12,13</sup>. For example, cooperative concerts through the Internet only require a moderate data rate but have a stringent requirement of low and stable latency. Low-order formats such as quadrature phase-shift keying should be used to provide a low bit error rate (BER) and forward error correction (FEC)-free signalling to minimize the latency and power consumption<sup>3</sup>. Remote education and remote work, however, require a high data rate to transmit high-resolution video with a relaxed tolerance to latency. Thus, higher-order formats such as 16-quadrature amplitude modulation (QAM) could be used<sup>14</sup>.

All these features should then be compatible with legacy infrastructures such as existing mobile fronthaul and passive optical networks, since the dominant cost in access networks is due to the fibre link deployment<sup>14</sup>.

Current user–cloud data transmission relies on time-division multiplexing (TDM) approaches through passive optical networks (for households and buildings)<sup>15</sup> or radio access networks (to base stations and radio units)<sup>16</sup>, with both employing tree-topology passive split fibre links for cost-efficient deployment. Scheduling and latency control in cloud-to-user data transmission (downstream) is relatively easy due to its broadcasting nature and the media access control layer protocols<sup>17</sup>. However, user–cloud (upstream) transmission presents a major challenge due to the random and bursty nature of data generated from the users. To avoid contention when multiple users simultaneously send their upstream data, current TDM systems use time scheduling and buffering of data frames with a large gap in between for user registration and dynamic bandwidth allocation (minimum 250  $\mu$ s due to protocols involving several two-way handshakes<sup>18</sup>), leading to an unavoidably large and unpredictable latency<sup>4</sup>. This negatively impacts the user experience, as well as creates potential risks for user safety in applications such as remote surgery and autonomous vehicles.

An alternative to the TDM approach is wavelength-division multiplexing (WDM)<sup>19</sup>, which offers dedicated bandwidth to each user and therefore promises guaranteed user–cloud communications with low and stable latency. The drawbacks that have prevented this technology from being implemented more widely are the high cost of WDM components (such as WDM routers and lasers of distinct wavelengths)

for every remote node and user, as well as the high operating expense due to the management/registration of the user wavelength. Combined WDM–TDM approaches<sup>20</sup> support more users with a lower cost than a WDM-only solution, but the use of TDM still leads to contention and queuing that precludes low and stable latency. Recently, electronic sub-carrier multiplexing (SCM) techniques using coherent transceivers have emerged to overcome these challenges and provide software-defined, bandwidth-flexible user–cloud connections<sup>14,21</sup>. However, these require expensive broadband ( $\geq 50$  GHz (ref. 14)) digital optical coherent transceivers with power-hungry application-specific integrated circuits for every user.

Furthermore, current access networks cannot provide scalable and low-cost time synchronization with sub-nanosecond accuracy, which is at the core of 6G and timing-critical applications<sup>22</sup>. Low-cost time synchronization protocols, such as the precision time protocol, only achieve microsecond accuracies due to the frequency deviation between device clocks<sup>23</sup>. A possible solution would be to implement rubidium atomic clocks, but equipping each user with such a high-cost, high-power-consumption device would be impractical.

A more viable solution is user device clock synchronization. This typically requires low-jitter clock frequency synchronization in conjunction with a clock-phase-tracking method. Key example approaches include White Rabbit<sup>24</sup> and clock phase caching<sup>25</sup>, both of which require a low-jitter frequency-synchronized clock signal, achieved either by recovering the clock frequency from data and performing clock jitter removal (for example, synchronous ethernet<sup>26</sup>) or the transmission of a dedicated clock signal<sup>25</sup>. Compared with synchronous ethernet, which causes up to 20 ns time error from the clock phase wander from the process of removing the high jitter from the data-distributed clock, low-jitter clock frequency synchronization via dedicated clock signals promises picosecond-level clock accuracy and therefore guaranteed performance. Nevertheless, although optical clock frequency synchronization has been successfully demonstrated in short-distance scenarios such as intra-data-centre networks, a scalable and low-cost technique to achieve low-jitter clock frequency synchronization is still lacking.

In this Article, we show that a closely spaced frequency-division multiplexing (FDM) method can provide dedicated bandwidth for every user, enabling contention-free, clock-synchronized user–cloud upstream communication. Although this is a WDM-only approach, it does not require expensive WDM components at the remote node and user side. Instead, the approach disseminates a frequency comb to all the users, which permits low-jitter clock frequency synchronization

**Table 1 | Future data rate and latency requirement for AR/VR devices and connected car fleet**

	VR	Connected car fleet
<b>Full view</b>	<b>Field of view</b>	
Data rate	Data rate	Data rate
<b>&gt;1.6 Gbps</b>	<b>&gt;870 Mbps</b>	<b>&gt;1 Gbps</b>
Latency	Latency	Latency
<b>&lt;2 ms</b>	<b>&lt;2 ms</b>	<b>&lt;3 ms</b>

Here the estimates for VR target the highest user experience with 24K resolution and a frame rate of 120 (ref. 4). Note that different VR devices and user experience standards are estimated to coexist in future deployment. Thus, the user transceivers must be flexible to support different data rates and formats. The estimates for the connected car fleet is obtained by considering 'AI drivers' user cases, where the car fleets exchange information including raw sensor data, vehicles' intention and coordination, enabling cooperative perception for AI drivers<sup>10</sup>. In contrast to conventional applications that predominantly require high bit rate for data transmission (for example, video streaming), the above time-critical applications require bounded low latency in conjunction with the ability to scale across a large number of consumer devices.

and optical carrier frequency synchronization using low-speed frequency locking, facilitating upstream FDM transmission over existing colourless passive power splitting fibre networks. It also does not require any modification of the deployed fibre infrastructure—that is, our FDM approach uses conventional deployed TDM networks—and is made practical by the maturity of technologies including frequency comb generation<sup>27,28</sup>, low-cost narrow-linewidth lasers<sup>29</sup>, laser frequency control<sup>30</sup> and digital optical coherent receiver techniques.

Our approach provides all the users with dedicated optical bandwidth for upstream data transmission without the need for time scheduling or data buffering, ensuring guaranteed and constant user connections with low and stable latency. The optical clock frequency dissemination approach provides low-jitter, scalable and low-cost clock frequency synchronization that leads to sub-nanosecond timing dissemination. Furthermore, the user transceivers only require low-speed electronic and optoelectronic components to transmit signals at the baseband. This reduces the cost and power consumption of the transceivers compared with the current TDM approach, which requires each user to operate at the full rate. For example, in a 50 Gbps TDM system<sup>18,31</sup>, each user requires a 25 Gbd transceiver, whereas the average per-user data rate is less than 800 Mbps (assuming 64 users).

We demonstrate frequency comb generation with more than five hundred 2.5-GHz-spaced tones with less than 10 dB power variation, providing clock synchronization to user transceivers with a  $\leq 4$  ps root-mean-square (r.m.s.) timing jitter (integrated over 1 kHz to 10 MHz) and a  $\leq 10$ -kHz-linewidth optical carrier. Using a low-cost frequency stabilization method, we report the FDM of 64 user signals with different modulation formats, promising up to 320 users with all the five demonstrated WDM bands. Up to 4.3 Gbps per-user data rate and a total capacity of 240.0 Gbps are achieved in a single 200 GHz WDM band, providing sufficient per-user data rate for time-critical applications.

## Clock- and frequency-referenced system architecture

At the core of our system is an optical frequency comb placed at the edge cloud, which is distributed to users/customers to provide them with both clock and optical carrier frequency references (Fig. 2a). The optical frequency comb is seeded by a narrow-linewidth laser to produce a low-noise optical frequency reference and the tone spacing is locked to a reference clock to enable clock distribution. The large number of optical frequency comb tones enables the FDM for a large number of users (for example, up to 320 users in this demonstration). The comb tones within the same WDM channel (for example, 100–200 GHz

bandwidth stated in the ITU-T standard) are routed to users in the same region (Fig. 2e), who are connected to the same passively split remote node. Each user uses a low-speed photodiode to detect the beatnote of the comb lines that provides a signal for their clock, which is detailed in the following section. Further, the users lock their transmitters to the assigned comb tones (one comb tone per user) and transmit their upstream signals within the designated optical bandwidth. This permits each user to have a dedicated optical bandwidth and synchronized clock for upstream transmission. Figure 2b shows the downstream comb after WDM demultiplexing and routing of each WDM channel to a group of users and Fig. 2c represents the aggregated upstream FDM signals from users using the same WDM channel.

The aggregated signals are detected and demodulated by a single broadband (160 GHz) optical coherent receiver at the edge data centre. Since the user signals are transmitted and detected within the designated optical bandwidth, the modulation formats and signal bandwidth can be flexibly adjusted to suit different traffic types without affecting other users. In our demonstration, we use low speed ( $4.9 \text{ GSa s}^{-1}$ ) and high-resolution (10 bit effective number of bits) digital-to-analogue converters (DACs) to generate SCM signals of different modulation formats. The electroabsorption modulators (EAMs) used have more than 5 GHz optoelectronic bandwidth, permitting adjustable bandwidth to suit different users' demands. Two example user cases are shown in Fig. 2e.

## Comb generator and clock phase noise

Our optical frequency comb generator and the experimental setup for clock and carrier distribution are shown in Fig. 3a. The optical frequency comb generator comprises a 10-kHz-linewidth seed laser followed by two comb generation stages. The first stage consists of an intensity modulator (IM) and two phase modulators (PMs) connected in tandem, all driven with in-phase 25 GHz radio-frequency (RF) signals to yield a 1.25-THz-bandwidth frequency comb with 5 dB spectral flatness (Fig. 3b). The second comb generator stage uses two cascaded IM and PMs, both driven with 2.5 GHz RF signals to convert each of the 25.0-GHz-spaced comb tones into a 2.5-GHz-spacing frequency comb with a spectral flatness of 6 dB. By locking the 25.0 GHz electronic phase-locked loop 1 (PLL<sub>1</sub>) with the 2.5 GHz PLL<sub>2</sub> to the same 10 MHz clock source, the 2.5 GHz comb signals generated from each 25.0-GHz-spacing tones are frequency and phase locked, yielding a 1.25-THz-bandwidth, 2.5-GHz-spacing comb signals with a spectral flatness better than 10 dB (Fig. 3c). The comb tones are subsequently amplified to 18 dBm using an erbium-doped fibre amplifier (EDFA) before being WDM demultiplexed into five 200 GHz WDM grid wavelength channels, each outputting 5 dBm optical power and containing approximately 70 tones (Fig. 3d). The WDM-demultiplexed comb tones are launched into 22 km of standard single-mode fibre (SSMF), which emulates the feeder fibre in the optical access links.

The distributed clock is recovered by detecting the comb beat using a 3-GHz-bandwidth photodiode followed by 40 dB RF amplification. The detected 2.5 GHz clock signal shows a clean spectrum (Fig. 3e) and is subsequently divided to 50 MHz (Fig. 3e, inset) and split to serve as the reference clock for all the user transceivers. We characterized the power budget for the distributed clock by attenuating the demultiplexed comb signals using a variable optical attenuator and calculating the r.m.s. timing jitter of the 50 MHz clock by integrating the measured phase noise from 1 kHz to 10 MHz. Using channel 4 (Fig. 3d, orange; 193.4–193.6 THz) as an example, the r.m.s. jitter remained below 4 ps with the optical power between  $-3$  and  $-18$  dBm. The abrupt increase in jitter when power drops to  $-17$  dBm was due to the failure of the frequency locking of the divider. The increased jitter with the high optical power is due to the saturation of the RF amplifiers. These results indicate more than 23 dB power budget available for clock dissemination, permitting a remote node split ratio of more than 64. Subsequently, we measured the phase noise and integrated

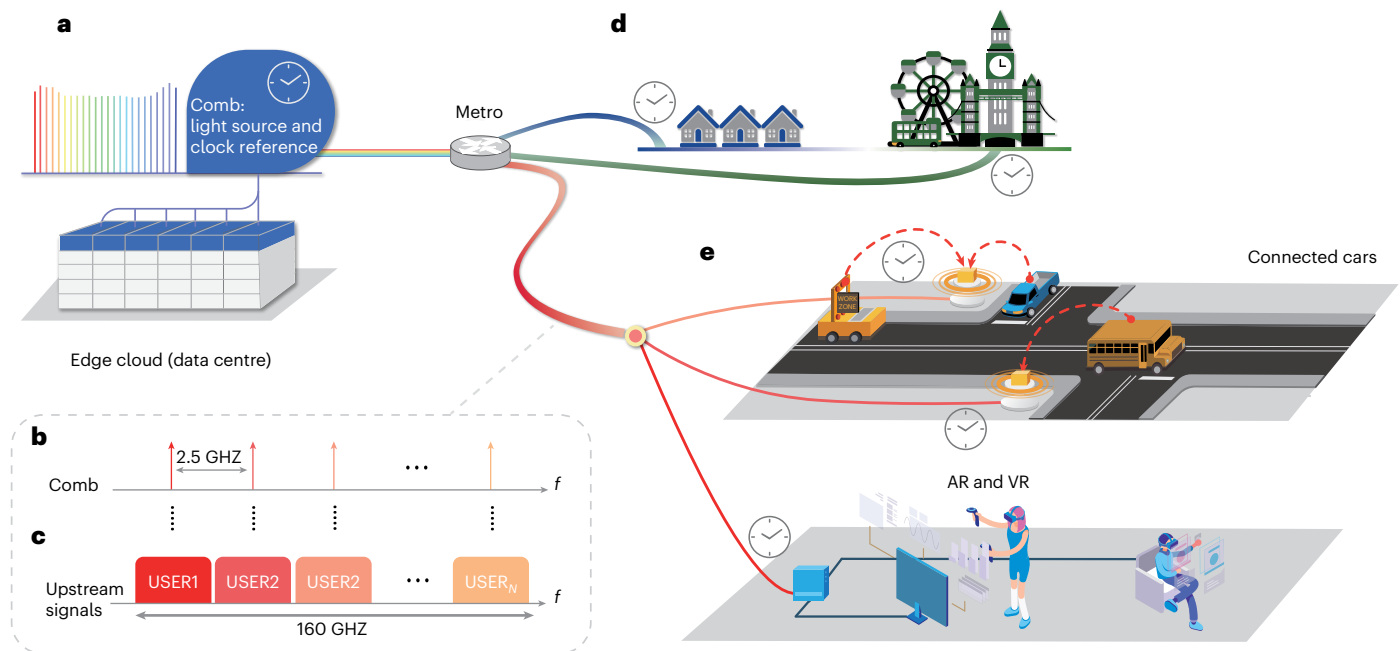


**Fig. 2 | Concept of clock- and optical-frequency-synchronized FDM upstream for time-critical applications.**

**a**, A wide-bandwidth closely spaced frequency comb generated at the edge cloud, referenced to a source clock within an edge data centre. **b**, Filtered frequency comb sent from an edge cloud or optical line terminal to the users. **c**, Upstream FDM signals; each user wavelength locked to

a selected tone in the distributed frequency comb, forming a wide-bandwidth optical signal that is detected by a single coherent receiver. **d**, Different WDM bands (for example, 100–200 GHz bandwidth) covers different passive split fibre networks. The blue, green and red colours indicate the different WDM bands. **e**, Exemplary time-critical applications including cooperative traffic system and VR.

jitter of the distributed clock for all the WDM channels at a received optical power of  $-13$  dBm. As shown in Fig. 3g, all the WDM channels show a sub-2 ps timing jitter, promising similar system performance over the whole wavelength region.

## FDM data aggregation

To demonstrate the FDM transmission, we carried out a series of experiments using a proof-of-concept system (Fig. 4a). Our system contains three live-user transceivers whose lasers are frequency locked to three neighbouring comb tones, resulting in three 2.5-GHz-spaced FDM signals after being combined by a coupler at the remote node (Fig. 4b shows the spectrum). The user transceivers are frequency synchronized to the optically distributed clock, eliminating any need for clock recovery at the coherent receiver side. We use the same type of single-wavelength lasers (about 150 kHz linewidth<sup>29</sup>) for all the transceivers. The continuous-wave (CW) signals from the lasers are split by a 50:50 coupler for frequency locking and upstream data transmission. To demonstrate the simultaneous detection of all the FDM signals within the same wavelength channel, we generate dummy signals by modulating the tapped comb signals after the 80 km decorrelation fibre (Fig. 4c, green). The aggregated upstream signals transmit back to the edge cloud side and are detected by a preamplified coherent receiver with 160 GHz optical bandwidth, centred at 193.407 THz (1,550.08 nm). The coherent receiver uses the seed laser wavelength filtered from the first-stage output as the local oscillator (LO). This not only provides the coherent receiver with a narrow-linewidth LO but also promises a deterministic frequency offset for user upstream signals, eliminating any dedicated carrier frequency offset (CFO) estimation module in the receiver digital signal processing (DSP). We subsequently measure the BER performance of the upstream SCM QAM signals. Different orders of QAM signals (4-/8-/16-QAM) with a root-raised-cosine pulse shape (roll-off factor of 0.01) are generated using the user transceivers' DACs.

To demonstrate the ability of each user to lock to any comb tone within the WDM channel (as required for flexible FDM channel

allocation), we tune the live users across the 160-GHz-frequency region (Methods). The live channels are always locked to the neighbouring comb tones and are combined with dummy signals to populate the 160 GHz bandwidth. Figure 4d shows the measured receiver sensitivities using live user1 as an example (Supplementary Section II provides details about the other two live users). At the soft-decision forward error code (SD-FEC) BER threshold of  $2 \times 10^{-2}$  (15.3% overhead<sup>32</sup>), the required lowest-power values are approximately  $-47$ ,  $-40$  and  $-35$  dBm for 4-/8-/16-QAM formats, respectively. The variation in sensitivity for different FDM channels is due to the high-frequency roll-off and imperfect impedance matching of the coherent receiver.

Since the user transceivers output about  $-4$  dBm, these results indicate a power budget of 43, 36 and 31 dB for an upstream per-user data rate of 2.14, 3.22 and 4.30 Gbps using 4-/8-/16-QAM signals, respectively. The relatively low output power was due to the high coupling loss of the used EAM in this experiment (about 10 dB). A potential 4–6 dB improvement in the power budget can be expected by using low-loss modulators such as the integrated EAM<sup>33</sup> or a Mach–Zehnder modulator<sup>34</sup>. In practice, different user branches may have varied losses due to the difference in component losses, fibre lengths and splitting ratio. We studied this by varying the power of the middle channel, which shows a linear relationship between the power and receiver sensitivity, indicating an amplified spontaneous emission (ASE) noise-limited performance (Supplementary Section III).

Considering a fully populated wavelength channel, the estimated aggregated data rates are about 133, 190 and 240 Gbps, using 4-/8-/16-QAM formats, respectively. The reduced power sensitivities at the edge of the optical bandwidth are primarily due to the frequency roll-off of the balanced photodiodes in the coherent receiver. Further, we study the frequency stability of the upstream user lasers. The minimum required power per tone for the frequency-locked loop (FLL) is  $-44$  dBm. At  $-35$  dBm power, the maximum frequency deviation is less than 1.5 MHz over 24 h (Fig. 4f). The stable frequency indicates that the



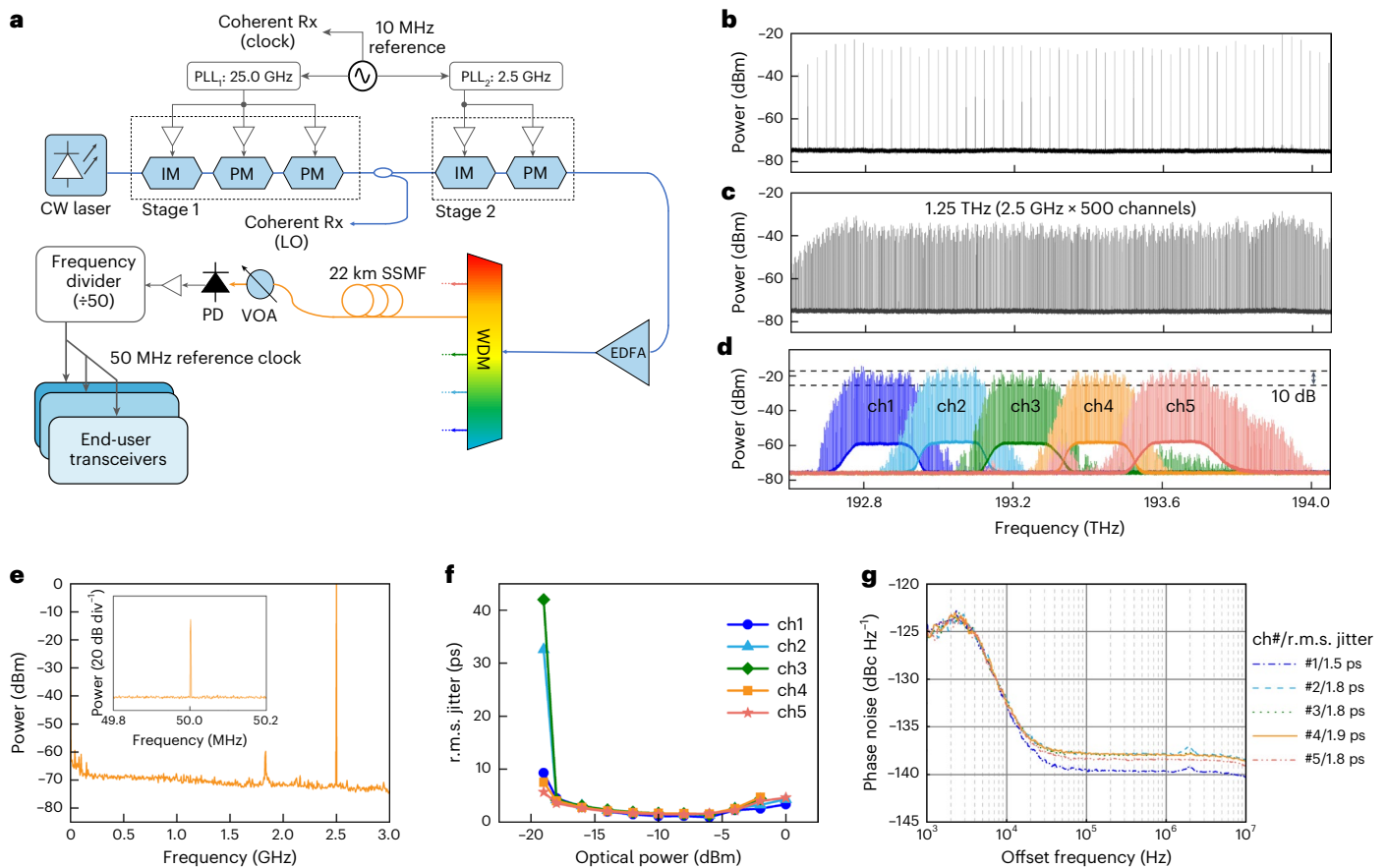


**Fig. 3 | Clock and carrier frequency distribution.** **a**, A CW laser seeds two stages of comb generator, yielding 1.25-THz-bandwidth 2.5-GHz-spacing comb signals with 10 dB flatness. The comb signals are sent to the end users for clock and carrier frequency synchronization. VOA, variable optical attenuator. **b**, Spectrum of the 25-GHz-spacing comb signals output from the first stage. **c**, Spectrum of the generated comb signal output from the second stage. **d**, Demultiplexed comb signals using a 200.0 GHz WDM each containing 64 tones of 2.5 GHz with about 10 dB spectral flatness. **e**, RF spectrum of the detected 2.5 GHz clock signal using channel 4 as an example (ITU ch35, 193.4–193.6 THz). **f**, Jitter of the

50 MHz reference clock for end-user transceivers at different received optical powers. The spur at around 1.8 GHz (about 60 dB below to the 2.5 GHz clock tone) is attributed to the slightly saturated RF amplifier, and it does not affect the phase noise as the divider that locks to the 2.5 GHz tone has <100 kHz loop bandwidth. The increased jitter value from -5 to 0 dBm is due to the saturation of the electronic amplifier and the decreased jitter value from -5 to -16 dBm is due to the reduced power. **g**, Measured phase noise of the distributed reference clock signals to different WDM channels, showing a maximum r.m.s. jitter of <2 ps, integrated over 1 kHz to 10 MHz.

system only requires a small guard band between the neighbouring channels for high spectral efficiency.

## Conclusions

A challenge for future digital infrastructure is how to provide guaranteed connections with low and stable latency for a large number of users. We identified that a bottleneck in optical access infrastructure to provide such services is the user–cloud upstream transmission and developed frequency-referenced multiplexing to enable guaranteed bandwidth and low latency. We limit our discussion to upstream in this Article, as downstream usually occupies different wave bands to avoid interference due to Rayleigh backscattering and parasitic reflections<sup>35</sup>.

Our approach generates a 2.5-GHz-space frequency comb using a two-stage configuration, which yields a low-noise, flat frequency comb with more than 500 tones to act as clock and optical frequency references. It disseminates the frequency comb to users through passive fibre networks, which provides clock and optical frequency synchronization for all the users, providing dedicated bandwidth for each user using low-cost and low-power-consumption electronics. As a proof of concept, we demonstrated an FDM system servicing up to 64 users with an aggregate bandwidth of 160 GHz, showing up to 4.3 Gbps per-user

data rate (240.0 Gbps per 200 GHz wavelength channel) with a high receiver sensitivity of -35 dBm.

Our demonstration uses 200-GHz-wavelength demultiplexers for each WDM channel, but smaller WDM channel bandwidth (for example, 100–160 GHz) could be used to fully utilize the available optical spectrum without any gap between the neighbouring WDM channels. This would increase the number of users to 500 by using multiple coherent receivers to detect signals from all the WDM channels. The number of users could be increased to more than 1,000 by using more wavelength channels within the low-loss telecommunications C band (for example, 1,540–1,562 nm). Wide-bandwidth flat spectra combs have been reported in this wavelength region using cascaded optoelectronic modulators<sup>27</sup>, optical parametric mixing<sup>28</sup> and a combination of both techniques<sup>36</sup>. Although the demonstrated frequency combs have more than 25 GHz tone spacing, they can be easily engineered to smaller spacing using a second stage. EDFAs with high and flat gain over the 1,535–1,565 nm wavelength region are readily available to ensure a sufficient power budget for clock and optical frequency synchronization. Further increase in the user numbers to a few thousand could benefit from the emerging ultrawideband transmission techniques, which have demonstrated lasers, flat-gain amplifiers and comb sources outside the telecom C band as well as more than 90 nm comb sources<sup>37</sup>.

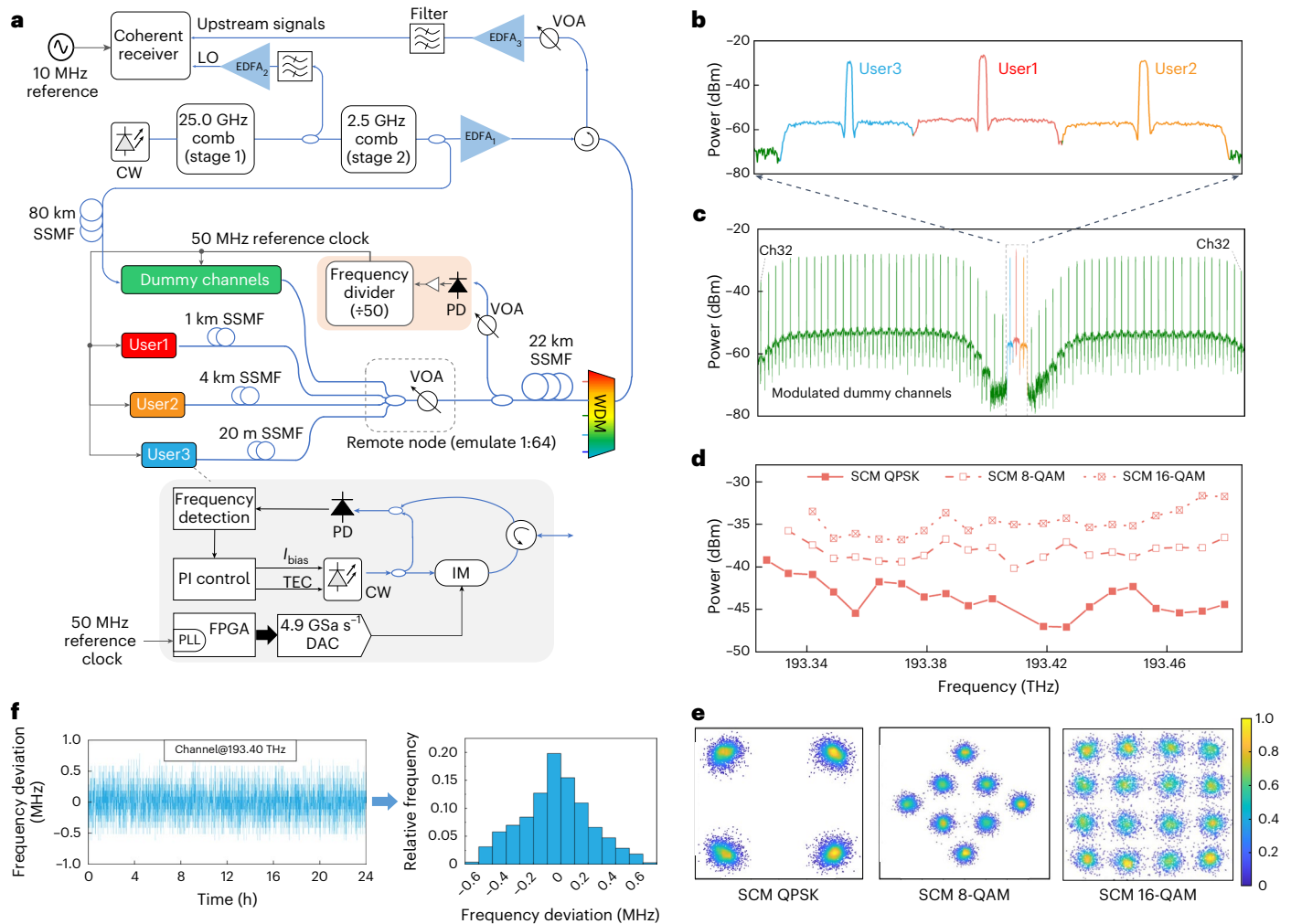


**Fig. 4 | Proof-of-concept experiment for the clock- and frequency-referenced FDM upstream data aggregation for time-critical applications.** **a**, System diagram of our proof-of-concept experiments with three live end users combined with dummy signals to form 160-GHz-optical-bandwidth signals. Due to the availability of components, the optically distributed clock is detected by a single photodiode and sent to all the live end-user transceivers via short coaxial cables as the clock reference. Based on the clock reference, three sets of field-programmable gate arrays (FPGAs) and 4.9 GSa s<sup>-1</sup> DACs generate SCM QAM signals and drive the corresponding IMs to generate the upstream signals. The user lasers generate CW signals with about 150 kHz linewidth and are frequency locked to neighbouring comb tones using an FLL containing a frequency detector and a PI controller, with about 10 kHz loop bandwidth. A thermoelectric

controller (TEC) provides feedback for long-term stability and coarse frequency tuning. Two couplers and a 10 dB attenuator are used to emulate 1:64 remote node splitting, resulting in a total link loss of about 28 dB (including 22 km SSMF loss, WDM loss and remote node splitting loss). **b**, Optical spectrum (20 MHz resolution) of the upstream signals received: red (user1), orange (user2) and blue (user3). Green indicates the modulated dummy channels. **c**, Optical spectrum (20 MHz resolution) of the combined upstream signals, with all the live transceivers locked to 2.5-GHz-spacing tones. **d**, Measured power sensitivity (power per user signal into EDFA3) for different modulation formats at the SD-FEC threshold of  $2 \times 10^{-2}$  (15.3% overhead): cross markers (4-QAM), open markers (8-QAM), closed markers (16-QAM). **e**, Measured constellation diagrams of user1. **f**, Measured frequency deviation over 24 h using user1 locked at 193.407 THz.

Our approach also reduces the RF bandwidth of user transceivers by a factor of  $N$  (where  $N$  is the number of users connected to the same remote node) compared with the conventional TDM approach. This leads to a reduction in power consumption and packaging costs, as well as enhanced jitter tolerance and fundamentally higher receiver sensitivities due to the reduced baud rate. The reduced user transceiver bandwidth also permits using high-resolution DAC that cannot be achieved in high-band-rate signalling<sup>38</sup>, enabling high-performance constellations or probabilistic-shaping DSP to improve the dynamic range and receiver sensitivity<sup>39</sup>. Besides offering flexible modulation formats, the bandwidth of each user can be further split into multiple sub-bands using digital sub-carrier modulation methods for optical wireless users<sup>40</sup>. The enhanced performance and flexibility offered in this system architecture creates new opportunities in software-defined networks that provide simpler and more efficient network resource allocation<sup>41</sup>.

As opposed to the optical PLL used in analogue coherent communications and metrology, where high-bandwidth optical PLLs are required to lock the optical phase<sup>42,43</sup>, our approach only requires stabilizing the user transceivers' frequency within a few megahertz of the designated comb tone. Thus, it requires only slow and low-cost feedback control. In this proof-of-concept work, the users' CW lasers are tuned to lock to different tones using thermoelectric controllers. In practice, the user transceivers should automatically lock to the assigned FDM channels. This could be achieved using network protocols or physical layer mechanisms.

Tunable lasers and laser control are typically considered to be too costly to implement in optical access networks. Although this is true for cost-sensitive optical access systems, our approach offers new features to ensure guaranteed bandwidth, low and stable latency and enhanced power budget (due to a low baud rate). Progress in laser material and

control electronics in the past decade has created possibilities to stabilize laser frequency in temperature-varying environments<sup>44</sup>. Compared with traditional WDM approaches that use lasers of distinct wavelengths, which require different designs and test procedures, our method allows for using the same type of laser for all the users. Thus, the cost could be brought down considerably with mass production.

The frequency comb, user transceivers and coherent receivers can be integrated on readily available InP photonic integration circuit platforms<sup>45</sup> and emerging heterogeneous integration platforms such as III–VI on silicon<sup>46</sup> and thin-film LiNbO<sub>3</sub> (ref. 47) promise low-cost and low-power-consumption devices and sub-systems. Besides the proposed user transceiver design, there are other potential alternatives using, for example, injection-locked lasers<sup>48</sup> or other narrowband amplification methods<sup>49</sup>, for tone selection and amplifications, which might be worth further investigation.

The narrow-linewidth laser and the reference clock that seed the comb generator can be synchronized to light sources and clocks in other data centres<sup>43</sup>, enabling global carrier frequency and clock synchronization over telecommunication networks for applications such as metrology, passive radar, radio astronomy and navigation<sup>50</sup>. Our clock frequency synchronization approach could be used in combination with clock phase tracking to achieve sub-nanosecond accuracy time synchronization<sup>51</sup>. Sub-nanosecond accuracy time synchronization of wireless access points, such as mobile network antennas, could then enable the positioning of wireless devices, such as connected car fleets and AR devices, to sub-30 cm accuracy<sup>22</sup>. Sub-nanosecond-accuracy of the time synchronization of mobile network antennas would also enable device positioning in environments that are difficult or impossible to achieve using GNSS technologies, such as underground, within buildings or within urban canyons<sup>22</sup>. Providing wide-coverage time synchronization through telecommunication networks would provide an alternative to the satellite-based clock dissemination systems (such as GPS) for emergency responses and recovery.

## Methods

### Comb generation and control

We use a RIO ORION laser emitting 13 dBm at 1,550.08 nm as the seed source. The CW light is amplified to 33 dBm before being modulated by two PMs and an IM driven with 25 GHz RF signals generated from a low-noise RF synthesizer (Rohde & Schwarz SMA100B). The RF signals that drive the PMs are amplified to 33 dBm, yielding a 25-GHz-spacing comb signal with 1.25 THz bandwidth (50 tones). The output of the first-stage comb generator is split into two branches. The upper branch is filtered and amplified as the LO of the coherent receiver, whereas the lower branch seeds the second-stage comb generator that consists of a PM and an IM. The PM in the second stage is driven with a 2.5 GHz RF signal with 30 dBm power. Both 25.0 GHz and 2.5 GHz RF signals are phase locked to the same 10 MHz reference clock. The generated 2.5-GHz-spacing comb signal has -10 dBm optical power and is subsequently amplified to 18 dBm using an EDFA.

### End-user transceivers

We implemented three live-user transceivers using the same model of single-wavelength low-cost lasers outputting an 8 dBm CW signal with about 150 kHz linewidth<sup>29</sup>. We used discrete mode lasers (EP1550 Narrow-Linewidth Series) that do not require regrowth in fabrication for low cost. The CW light was split by a 50:50 coupler and mixed with the downstream frequency comb to generate a beatnote corresponding to the frequency difference between the CW and the selected reference tone for feedback current control, using a proportional–integral (PI) controller. The frequency discriminator is based on analogue electronic PLL with 6 MHz locking range. A polarization controller was used to align the lasers' output to the selected comb tone. This, however, can be eliminated by using an integrated polarization tracker or polarization scrambling of the comb signal.

The EAMs have a 10 dB insertion loss and an extinction ratio of more than 10 dB. They are driven with 1.072 GBaud SCM QAM signals, generated using 4.9 GSa s<sup>-1</sup> DACs. The digital SCM QAM signals were generated offline using a pseudorandom binary sequence of 2<sup>15</sup> length, mapped to QAM symbols, shaped by a root-raised-cosine filter with a roll-off factor of 0.01, and upconverted to a carrier frequency of 0.635 GHz to generate real-value SCM QAM signals. This allows for a 0.1 GHz gap between the d.c. and SCM signals in the generated large-carrier double-side-band signal. The resultant baseband bandwidth equals 1.165 GHz, which indicates that only 1.250-GHz-class optoelectronics components are required. The frequency and phase noise can be directly estimated from the carrier<sup>52,53</sup> in the receiver DSP, precluding complex CFO and carrier phase estimation algorithms.

The dummy channels were generated by modulating the tapped reference comb signals after transmission through an 80 km SSMF for decorrelation. The decorrelated comb passes through a waveshaper used as a tunable notch filter before combining with the live signals to form the 160-GHz-bandwidth upstream signals (Supplementary Section IV). The power roll-off of the channels next to the live channels is due to the limited bandwidth resolution (10 GHz) of the waveshaper, which also resulted in a limited (about 25 dB) power suppression in the centre of the notch filter. The middle channel is reported as the main performance indicator since the interchannel interference is primarily due to the neighbouring channels. The dummy channels are modulated by a Mach–Zehnder modulator driven with 1.072 GBaud intensity-modulated SCM 4-QAM signals with a carrier-to-signal-power ratio of about 14 dB, which is similar to that of the live signals. The frequency stability is measured by calculating the spectra of the beatnote waveforms.

### Coherent receiver and DSP

The upstream signals are preamplified using an EDFA (5 dB noise figure), filtered and detected by a 70-GHz-bandwidth dual-polarization coherent receiver. The waveforms were subsequently captured by a 100-GHz-bandwidth 256 GSa s<sup>-1</sup> real-time oscilloscope before performing offline DSP, in which the three user channels were demodulated. The coherent receiver is referenced to the same 10 MHz clock source as the frequency comb generator. Thus, the coherent receiver and user transceivers are frequency synchronized with low jitter. Since the two-sample-per-symbol equalizer is insensitive to the sampling clock phase, no clock-recovery DSP is used. In addition, no dispersion compensation was required due to the low baud rate per user. Since the frequency offset between the user channel and LO is known, the received live-user signals are downconverted to the baseband without needing CFO estimation. The residual CFO and optical phase are recovered by a phase-noise-recovery DSP module enabled by the large beat carrier (Supplementary Section V provides the performance details)<sup>52,53</sup>. The downconverted user signals are match filtered and equalized by a pre-trained Volterra filter. The Volterra equalizer with memory lengths of 13 and 9 for the linear and third-order Volterra kernels, respectively, has a negligible effect on the transceiver DSP latency since it is feedforward and multiplications can be computed in parallel, whose computing complexity could be optimized via various constraint criteria<sup>54</sup>. The tap coefficient of the Volterra filter is pretrained and can be stored for individual channels to reduce the processing latency. The BER results for the live-user signals are measured using 400,000 bits. The sensitivities for the SD-FEC threshold are estimated from the BER curves using linear interpolation (Supplementary Fig. 1). Supplementary Section V provides the DSP function blocks.

### BER and sensitivity characterization

The sensitivities (Fig. 4d) are calculated from the BER measurement for live user1. The BER values are measured by varying the optical power into EDFA<sub>3</sub> using a variable optical attenuator (Fig. 3a). The power per user channel was measured using an optical spectrum analyser of



0.01 nm resolution. Each BER value is calculated using a pseudorandom binary sequence of  $2^{15}$  length. Supplementary Section I provides the detailed BER results for all the live users. The aggregated capacity is calculated by multiplying the end-user data rate with a number of channels, achieving sub-SD-FEC BER. With 4-/8-/16-QAM, 62, 59 and 56 channels can achieve sub-SD-FEC BER, respectively. With wide-bandwidth coherent receivers, the aggregated data rate could be further improved to 275 Gbps using SCM 16-QAM for all the 64 users.

## Data availability

The data that supports the figures within this paper are available via figshare at <https://doi.org/10.5522/04/19653351>. Source data are provided with this paper.

## References

- European Technology Platform Network 2020. Smart networks in the context of NGL. *Strategic Research and Innovation Agenda 2021-27. Network Public* (2020); <https://www.networkdeurope.eu/3487-2/>
- Agrell, E. et al. Roadmap of optical communications. *J. Opt.* **18**, 063002 (2016).
- Dohler, M. et al. Internet of skills, where robotics meets AI, 5G and the tactile Internet. In *European Conference on Networks and Communications (EuCNC)* 1–5 (IEEE, 2017).
- Huawei iLab Ultimate Experience. *Cloud VR Network Solution White Paper* (Huawei iLab, 2018).
- Willars, P. et al. *Enabling Time-Critical Applications over 5G with Rate Adaptation* (Ericsson–Deutsche Telekom, 2021).
- Bonk, R. & Pfeiffer, T. New use cases for PONs beyond residential services. In *Optical Fiber Communication Conference Tu2G-1* (Optica, 2022).
- ResearchAndMarkets.com. Autonomous driving high-precision positioning: 2018-2019 industry report. *BusinessWire* <https://www.businesswire.com/news/home/20190311005756/en/Autonomous-Driving-High-Precision-Positioning-2018-2019-Industry-Report—ResearchAndMarkets.com> (11 March 2019).
- Cui, Y. & Ge, S. S. Autonomous vehicle positioning with GPS in urban canyon environments. *IEEE Trans. Robot. Autom.* **19**, 15–25 (2003).
- Mehmood, M., Saleem, S. & Filjar, R. Eyjafjallajökull volcanic ash 2010 effects on GPS positioning performance in the Adriatic Sea region. *Atmosphere* **13**, 47 (2021).
- Sakaguchi, K. et al. Towards mmWave V2X in 5G and beyond to support automated driving. *IEICE Trans. Commun.* **104**, 587–603 (2020).
- 3GPP 5G. Service requirements for enhanced V2X scenarios (TS 22.186 version 15.3.0 Release 15) (2018).
- Bogdoll, D. et al. Kiglis: smart networks for smart cities. In *IEEE International Smart Cities Conference (ISC2)* 1–4 (IEEE, 2021).
- Kizilkaya, B., Zhao, G., Sambo, Y. A., Li, L. & Imran, M. A. 5G-enabled education 4.0: enabling technologies, challenges, and solutions. *IEEE Access* **9**, 166962–166969 (2021).
- Welch, D. et al. Point-to-multipoint optical networks using coherent digital subcarriers. *J. Light. Technol.* **39**, 5232–5247 (2021).
- G.989.2. 40-gigabit-capable passive optical networks 2 (NG-PON2): physical media dependent (PMD) layer specification—amendment 1 (2020); <https://www.itu.int/rec/T-REC-G.989.2>
- Bidkar, S., Bonk, R. & Pfeiffer, T. Low-latency TDM-PON for 5G Xhaul. In *International Conference on Transparent Optical Networks (ICTON)* 1–4 (IEEE, 2020).
- eCPRI specification v2.0 (2019); [http://www.cpri.info/downloads/eCPRI\\_v\\_2.0\\_2019\\_05\\_10c.pdf](http://www.cpri.info/downloads/eCPRI_v_2.0_2019_05_10c.pdf)
- G.9807.1. 10-gigabit-capable symmetric passive optical network (XGS-PON) (2016); [https://www.itu.int/rec/dologin\\_pub.asp?lang=e&id=T-REC-G.9807.1-201606-1!!PDF-E&type=items](https://www.itu.int/rec/dologin_pub.asp?lang=e&id=T-REC-G.9807.1-201606-1!!PDF-E&type=items)
- Grobe, K. & Elbers, J.-P. PON in adolescence: from TDMA to WDM-PON. *IEEE Commun. Mag.* **46**, 26–34 (2008).
- Luo, Y. et al. Time- and wavelength-division multiplexed passive optical network (TWDM-PON) for next-generation PON stage 2 (NG-PON2). *J. Light. Technol.* **31**, 587–593 (2012).
- Lavery, D. et al. A 32x10 Gb/s OLT using a single ultra-wide bandwidth dual local oscillator coherent receiver. In *IEEE Photonics Conference (IPC) Part II 1–2* (IEEE, 2017).
- Koelemeij, J. et al. A hybrid optical-wireless network for decimetre-level terrestrial positioning. *Nature* **611**, 473–478 (2022).
- IEEE 1588-2019. IEEE standard for a precision clock synchronization protocol for networked measurement and control systems (2019); <https://standards.ieee.org/ieee/1588/6825/>
- Lipiński, M., Włostowski, T., Serrano, J. & Alvarez, P. White Rabbit: a PTP application for robust sub-nanosecond synchronization. In *2011 IEEE International Symposium on Precision Clock Synchronization for Measurement, Control and Communication* 25–30 (IEEE, 2011).
- Clark, K. et al. Synchronous subnanosecond clock and data recovery for optically switched data centres using clock phase caching. *Nat. Electron.* **3**, 426–433 (2020).
- G.8261. Timing and synchronization aspects in packet networks (2008); <https://www.itu.int/rec/T-REC-G.8261>
- Torres-Company, V. & Weiner, A. M. Optical frequency comb technology for ultra-broadband radio-frequency photonics. *Laser Photon. Rev.* **8**, 368–393 (2014).
- Kuo, B. P.-P. et al. Wideband parametric frequency comb as coherent optical carrier. *J. Light. Technol.* **31**, 3414–3419 (2013).
- O’Carroll, J. et al. Wide temperature range  $0 < T < 85^{\circ}\text{C}$  narrow linewidth discrete mode laser diodes for coherent communications applications. *Opt. Express* **19**, B90–B95 (2011).
- Feng, Z. et al. Comb-locked telecom-grade tunable laser using a low-cost FPGA-based lockbox. In *Conference on Lasers and Electro-Optics (CLEO) STu1J-4* (IEEE, 2021).
- Rosales, R. et al. Achieving high budget classes in the downstream link of 50G-PON. *J. Opt. Commun. Netw.* **13**, D13–D21 (2021).
- Miyata, Y. et al. UEP-BCH product code based hard-decision FEC for 100 Gb/s optical transport networks. In *Optical Fiber Communication Conference JW2A-7* (Optica, 2012).
- Trajkovic, M., Blache, F., Debregeas, H., Williams, K. A. & Leijtens, X. J. Increasing the speed of an InP-based integration platform by introducing high speed electroabsorption modulators. *IEEE J. Sel. Topics Quantum Electron.* **25**, 3400208 (2019).
- Li, K. et al. Electronic–photonic convergence for silicon photonics transmitters beyond 100 Gbps on–off keying. *Optica* **7**, 1514–1516 (2020).
- Zhang, D., Liu, D., Wu, X. & Nettet, D. Progress of ITU-T higher speed passive optical network (50G-PON) standardization. *J. Opt. Commun. Netw.* **12**, D99–D108 (2020).
- Sohanpal, R. et al. All-fibre heterogeneously-integrated frequency comb generation using silicon core fibre. *Nat. Commun.* **13**, 3992 (2022).
- Puttnam, B. J. et al. S, C and extended L-band transmission with doped fiber and distributed raman amplification. In *Optical Fiber Communications Conference and Exhibition (OFC) Th4C-2* (IEEE, 2021).
- Clara, M. *High-Performance D/A Converters: Application to Digital Transceivers* Vol. 36 (Springer Science & Business Media, 2012).
- Xing, S. et al. First demonstration of PS-QAM based flexible coherent PON in burst-mode with 300G peak-rate and record dynamic-range and net-rate product up to 7,104 DBGbps. In *Optical Fiber Communication Conference Th4A-4* (Optica, 2022).



40. Lavery, D. et al. Opportunities for optical access network transceivers beyond OOK. *J. Opt. Commun. Netw.* **11**, A186–A195 (2019).
41. Luo, Y., Gao, L. & Huang, J. MINE GOLD to deliver green cognitive communications. *IEEE J. Sel. Areas Commun.* **33**, 2749–2760 (2015).
42. Balakier, K., Ponnampalam, L., Fice, M. J., Renaud, C. C. & Seeds, A. J. Integrated semiconductor laser optical phase lock loops. *IEEE J. Sel. Topics Quantum Electron.* **24**, 1500112 (2017).
43. Brodnik, G. M. et al. Optically synchronized fibre links using spectrally pure chip-scale lasers. *Nat. Photon.* **15**, 588–593 (2021).
44. Blumenthal, D. J. et al. Frequency stabilized lasers for coherent fiber interconnects in the datacenter (invited talk). In *2019 IEEE Optical Interconnects Conference (OI)* 1–2 (IEEE, 2019).
45. Smit, M., Williams, K. & Van Der Tol, J. Past, present, and future of InP-based photonic integration. *APL Photon.* **4**, 050901 (2019).
46. Doerr, C. & Chen, L. Silicon photonics in optical coherent systems. *Proc. IEEE* **106**, 2291–2301 (2018).
47. Xu, M. et al. High-performance coherent optical modulators based on thin-film lithium niobate platform. *Nat. Commun.* **11**, 3911 (2020).
48. Liu, Z. & Slavik, R. Optical injection locking: from principle to applications. *J. Light. Technol.* **38**, 43–59 (2020).
49. Giacomidis, E. et al. Chip-based Brillouin processing for carrier recovery in self-coherent optical communications. *Optica* **5**, 1191–1199 (2018).
50. Riehle, F. Optical clock networks. *Nat. Photon.* **11**, 25–31 (2017).
51. Clark, K., Zhou, Z. & Liu, Z. Picosecond-precision clock synchronized radio access networks using optical clock distribution and clock phase caching. In *Optical Fiber Communication Conference and Exhibition (OFC) W4F-3* (IEEE, 2023).
52. Liu, Z., Kim, J.-Y., Wu, D. S., Richardson, D. J. & Slavik, R. Homodyne OFDM with optical injection locking for carrier recovery. *J. Light. Technol.* **33**, 34–41 (2015).
53. Jansen, S. L., Morita, I., Schenk, T. C. W., Takeda, N. & Tanaka, H. Coherent optical 25.8-Gb/s OFDM transmission over 4160-km SSMF. *J. Light. Technol.* **26**, 6–15 (2008).
54. Wettlin, T. et al. Complexity reduction of Volterra nonlinear equalization for optical short-reach IM/DD systems. In *Photonic Networks; 21th ITG-Symposium* 1–6 (VDE, 2020).
55. Morrish, J. Human machine interface 101: a primer on new emerging AR and VR techniques that enable human interaction with new emerging technical environments (Transforma Insights, 2021).
56. PwC and Strategy&. *The 2021 Digital Auto Report (Volume 1)—Assessing Global Mobility Market Dynamics* (PwC and Strategy&, 2021).

## Acknowledgements

Z.L. acknowledges financial support from EPSRC grants ORBITS (EP/V051377/1), programme grant TRANSNET (EP/R035342/1) and the strategical equipment grant (EP/V007734/1). Z.L., Z.Z. and K.A.C. acknowledge the ATOM project (10037307) funded by the Innovate UK National Timing Centre. K.A.C. acknowledges the Royal Academy of Engineering (RF2122-21-234). R.S. acknowledges EPSRC Doctor Training Centre EP/L015455/1 for funding the PhD study. C.D. acknowledges EPSRC NPIF doctoral training (EP/R512400/1). R.S. acknowledges EPSRC programme grant AirGuide Photonics (EP/P030181/1). J.W. acknowledges the major key project of PCL

(no. PCL2021A17). Y.L. acknowledges the National Natural Science Foundation of China (Project 62102343), Shenzhen Key Lab of Crowd Intelligence Empowered Low-Carbon Energy Network (no. ZDSYS20220606100601002) and the Shenzhen Institute of Artificial Intelligence and Robotics for Society.

## Author contributions

Z.L., Y.L., Z.Z. and K.A.C. prepared the manuscript. Z.L. and J.W. conceived the frequency-referenced user multiplexing system architecture. Z.L. and Y.L. conceived the clock and frequency dissemination approach. K.C., R.Slavik and Z.L. developed and implemented the transceivers. C.D., R.Sohanpal, Z.Z. and Z.L. developed the frequency comb source. Z.Z. and C.D. contributed to the phase noise and jitter characterizations. Z.Z. developed the clock synchronization sub-systems and characterized their performance. Z.Z. and Z.L. performed the experiments, including BER and power sensitivity testing, stabilization of the user lasers, signal generation, coherent detection and associated performance characterization. E.S. contributed to coherent signal detection. Z.L., J.W. and Y.L. developed the core digital signal processing. All authors contributed in analysing the experimental results. Z.L. supervised and led the scientific collaboration.

## Competing interests

The authors declare no competing interests.

## Additional information

**Supplementary information** The online version contains supplementary material available at <https://doi.org/10.1038/s41928-023-01022-x>.

**Correspondence and requests for materials** should be addressed to Jinlong Wei, Yuan Luo or Zhixin Liu.

**Peer review information** *Nature Electronics* thanks Xingjun Wang and the other, anonymous, reviewer(s) for their contribution to the peer review of this work.

**Reprints and permissions information** is available at [www.nature.com/reprints](http://www.nature.com/reprints).

**Publisher's note** Springer Nature remains neutral with regard to jurisdictional claims in published maps and institutional affiliations.

**Open Access** This article is licensed under a Creative Commons Attribution 4.0 International License, which permits use, sharing, adaptation, distribution and reproduction in any medium or format, as long as you give appropriate credit to the original author(s) and the source, provide a link to the Creative Commons license, and indicate if changes were made. The images or other third party material in this article are included in the article's Creative Commons license, unless indicated otherwise in a credit line to the material. If material is not included in the article's Creative Commons license and your intended use is not permitted by statutory regulation or exceeds the permitted use, you will need to obtain permission directly from the copyright holder. To view a copy of this license, visit <http://creativecommons.org/licenses/by/4.0/>.

© The Author(s) 2023